PARTONS AND SMALL X*

A.D. MARTIN

Department of Physics, University of Durham, England
and
H. Niewodniczański Institute of Nuclear Physics
Kraków, Poland

(Received November 29, 1993)

We review recent developments concerning the partonic structure of the proton. We describe a recent parton distribution analysis which incorporates the new precision deep inelastic scattering and related data. We discuss the application of perturbative QCD in the small x regime which is currently being probed, for the first time, by the experiments at HERA. We introduce, and consider applications of, the BFKL equation. We summarize the status of parton shadowing calculations. We briefly discuss implications of the new polarized neutron structure function measurements.

PACS numbers: 12.38. Bx, 12.38. Qk, 13.60. Hb

1. Introduction

The precise determination of the partonic structure of the proton is important, since the parton densities are universal and are essential ingredients in the detailed study of any hard interaction involving a proton. The distributions are determined by the values of the structure functions $F_i(x,Q^2)$ measured in muon (or electron)-nucleon (or nucleus) and neutrino-nucleus deep-inelastic scattering experiments, as well as by data from other related processes. For example, the relation between the observable structure function $F_2^{\mu p}$ and the parton densities f_i is of the form

$$F_2^{\mu p}(x,Q^2) = \sum_{i=q,\bar{q}} e_q^2 x f_q(x,Q^2) + \alpha_s(Q^2) \sum_{i=q,\bar{q},g} x \int_x^1 \frac{dz}{z} c_i(z) f_i(\frac{x}{z},Q^2), \tag{1}$$

* Presented at the XXXIII Cracow School of Theoretical Physics, Zakopane, Poland, June 1-11, 1993.

at next-to-leading order in α_s, where the coefficients $c_i(z)$ are known, but scheme dependent, functions. As usual x and Q^2 are independent invariant variables that can be constructed from the 4-momenta of the proton, p, and the probe, q; that is $Q^2 \equiv -q^2$ and $x = -q^2/p\cdot q$, see Fig. 1. Fig. 1 displays possible partonic structure of the proton as seen by the probe, q. Recall that x is equal to the fraction of the proton's momentum that is carried by the struck (massless) quark.

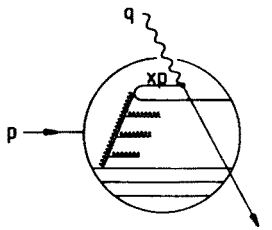

Fig. 1. Possible partonic structure of the proton as seen by a probe of 4-momentum q. The struck quark carries a fraction x of the proton's momentum. The gluon chain may contain quark links, particularly at large x.

Recent fixed-target deep-inelastic scattering data from NMC [1] and the CCFR collaboration [2] have considerably improved our knowledge of the parton distributions. Indeed the global description of these, and other related, data in terms of a set of universal parton densities provides an impressive confirmation of perturbative QCD. However it is the results that are just starting to come from the electron-proton collider, HERA, that are causing excitement. The reason is that HERA is probing the previously unexplored small x regime ($x \sim 10^{-3}$) where novel perturbative QCD effects are anticipated. The application of perturbative QCD in this region requires a resummation of $\alpha_s \log(1/x)$ terms, corresponding to the sum over gluon chains like the one shown in Fig. 1. To leading order this is accomplished by the BFKL equation [3] and leads to a singular small x behaviour of the gluon distribution of the form

$$xg \sim x^{-\lambda}, \tag{2}$$

where $\lambda \approx 0.5$, and similarly for the sea quark distributions since they are driven by the gluon, via $g \to q\bar{q}$. This behaviour is stable to evolution in Q^2 and thus the QCD expectation at small x is that

$$F_2^{ep}(x, Q^2) \sim x\bar{q} \sim x^{-0.5}. \tag{3}$$

This singular behaviour must eventually, as x decreases, be tamed by shadowing. The rise of F_2, with decreasing x, observed by H1 [4] and ZEUS [5]

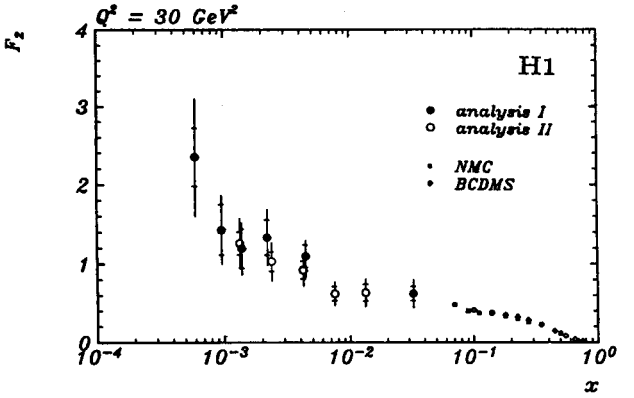

Fig. 2. The new measurements of $F_2^{\mu p}$ by NMC [1] and of F_2^{ep} at HERA [4], together with previous BCDMS [6] data. ZEUS [5] obtain similar results in the HERA range. At lower Q^2 values the NMC values reach down to $x \sim 10^{-2}$. The figure is taken from the CERN Courier, October 1993.

at HERA is perhaps the first evidence of this singular behaviour. Typical new experimental developments for F_2 are shown in Fig. 2.

2. Determination of parton distributions

The parton densities $f_i(x, Q^2)$ at some scale must be determined by experiment. The basic procedure is to parametrize the x dependence of $f_i(x, Q^2)$ at some low Q_0^2 but where Q_0^2 is sufficiently large for perturbative QCD to be applicable. Then to evolve up in Q^2 using next-to-leading order Altarelli–Parisi equations to determine $f_i(x, Q^2)$ at all values of x and Q^2 where deep-inelastic and related data exist, and in this way to perform a global fit to the data.

The deep-inelastic muon and neutrino data pin down the valence and sea quark distributions, but hardly constrain the gluon distribution, which only enters directly at next-to-leading order; essentially the only constraint is the momentum sum rule which shows that the gluon carries just less than 50% of the proton's momentum at Q_0^2. On the other hand the gluon enters at leading order in prompt photon production. Indeed for "large" p_T photons, produced by $pp \to \gamma X$, the dominant QCD subprocess is $gq \to \gamma q$, in contrast to $p\bar{p} \to \gamma X$ where the annihilation process $q\bar{q} \to \gamma g$ is much more important. The relevant data are from the WA70 collaboration [7] which determine the gluon for $x \sim 0.35$. Combined with the momentum sum

rule constraint, the global fit [8] is found to give an input gluon behaviour $(1-x)^{5.3}$ at large x. Data for the Drell–Yan $pN \to \mu^+\mu^- X$ process, which at leading order is mediated by $q_v\bar{q}_{\rm sea} \to \gamma^*$, constrain the $(1-x)^{\eta_s}$ behaviour of the sea quark distributions. Measurements of W production at $\bar{p}p$ colliders impose tight constraints on the u and d distributions, particularly when the accurate NMC measurements of $F_2^{\mu n}/F_2^{\mu p}$ have to be fitted simultaneously.

To be specific we present the latest MRS analysis [9, 8]. The input parametrizations at $Q^2 = Q_0^2$ $(= 4\ {\rm GeV}^2)$ of the gluon (g), valence (u_v, d_v) and sea $(\bar{u} = \bar{d} \simeq 2\bar{s})$ quark distributions each are assumed to have the form

$$x f_i(x, Q_0^2) = A_i x^{-\lambda_i}(1-x)^{\beta_i}(1 + \gamma_i x^{1/2} + \delta_i x)\,, \qquad (4)$$

where $u \equiv f_u = u_v + u_{\rm sea}$, $\bar{u} = u_{\rm sea}$ *etc.* and where the parameters $A_i, \lambda_i, \beta_i, \gamma_i, \delta_i$ are to be determined by the fit to the data. In practice not all these parameters are free. Three of the A_i are determined by the flavour and momentum sum rules. Moreover we have some idea of the values of λ_i and β_i from the expected behaviour of the parton distributions as $x \to 0$ and $x \to 1$ respectively. Naive counting rule estimates suggest $\beta_i \simeq 2n_s - 1$ where n_s is the minimum number of spectator partons accompanying the probed parton. So for valence quarks, gluons and sea quarks we expect β_i to be 3, 5 and 7 respectively. Naive Regge arguments suggest $\lambda_{i=v} \simeq \alpha_M(0) - 1 \simeq -0.5$ since in this model the $x \to 0$ (*i.e.* $p\cdot q \to \infty$) behaviour of the valence quarks distributions is controlled by the intercept $\alpha_M(0)$ of the (leading) $\rho - a_2 - \omega - f_2$ meson Regge trajectory. On the other hand $\lambda_{\rm sea} \simeq \lambda_g \simeq \alpha_P(0) - 1 \simeq 0$ if we assume that the Pomeron has intercept about 1. However we have mentioned that there are theoretical reasons from perturbative QCD to believe $\lambda_{\rm sea} \simeq \lambda_g \simeq 0.5$. We must therefore distinguish the "soft" pomeron (applicable in the Regge domain, $Q^2 \approx 0$) from the "hard" or "BFKL" pomeron (applicable at Q^2 values where perturbative QCD is valid). To illustrate the difference MRS obtain parton sets with $\lambda_g = \lambda_{\rm sea} = 0$ (sets $\rm D_0$ and $\rm S_0$) and a set with $\lambda_g = \lambda_{\rm sea} = 0.5$ (set $\rm D_-$).

Let us return to the input assumption that the sea quark distributions[1] satisfy $\bar{u} = \bar{d} = 2\bar{s}$. The evidence that the strange sea is about half as weak as the non-strange seas comes from the observations of deep-inelastic dimuon production, $\nu N \to \mu^-\mu^+ X$, for which the dominant subprocess is $\nu s \to \mu^-(c \to \mu^+)$. The latest CCFR [12] next-to-leading order analysis is shown in Fig. 3 and indicates that the MRS assumption for $\bar{s}$ is satisfactory.

[1] CTEQ [10] use freely parametrized input distributions for $\bar{u}$, $\bar{d}$ and $\bar{s}$. A critique of this approach (which yields an unphysically large strange sea distribution for $x \sim 0.05$) is given in Ref. [11], see also Fig. 3.

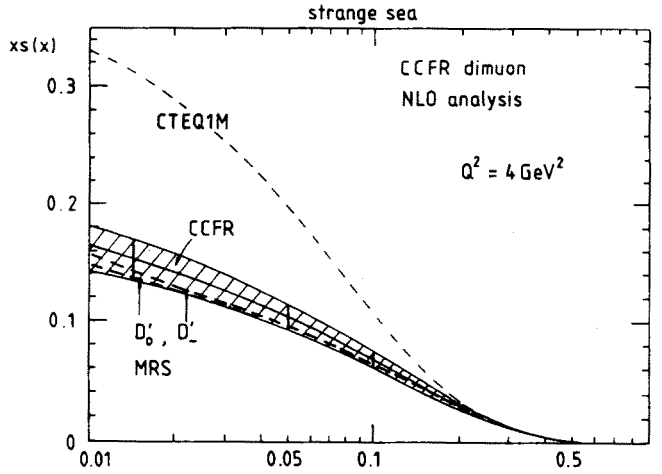

Fig. 3. The shaded band shows the strange quark distribution extracted by CCFR from their dimuon data [12], together with the MRS [8] and CTEQ [10] distributions.

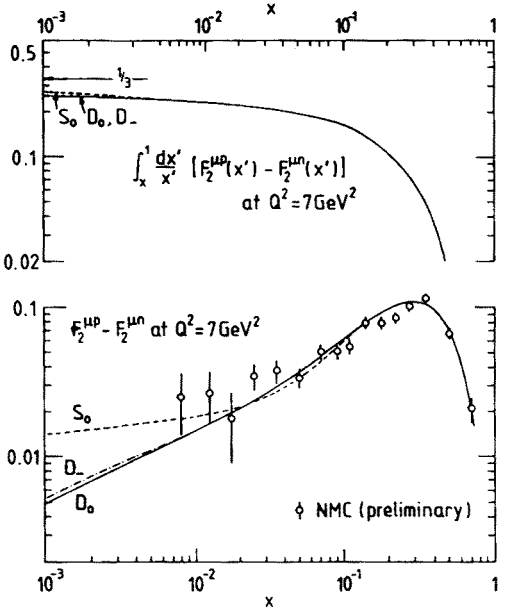

Fig. 4. The upper curves are the accumulated contribution, $\int_x^1$, to the Gottfried sum rule, (6), as a function of x, the lower limit of integration, corresponding to partons sets S_0, D_0 and D_- [9]. The lower curves compares the integrand, $F_2^{\mu p} - F_2^{\mu n}$, with NMC data [13].

Until recently all global analyses assumed $\bar{u} = \bar{d}$, but recent NMC data [13] imply that this equality may not be exact. This is best seen in terms

of the Gottfried sum rule

$$I_{\rm GSR} \equiv \int_0^1 \frac{dx}{x}(F_2^{\mu p} - F_2^{\mu n}) = \tfrac{1}{3}\int_0^1 dx(u_v - d_v) + \tfrac{2}{3}\int_0^1 dx(\bar{u} - \bar{d}) = \tfrac{1}{3}\,, \quad (6)$$

if $\bar{u} = \bar{d}$. On the other hand NMC [13] find

$$\int_{0.004}^{0.8} \frac{dx}{x}(F_2^{\mu p} - F_2^{\mu n}) = 0.236 \pm 0.016\,, \quad (7)$$

at $Q^2 = 4$ GeV^2. A straightforward comparison of (6) and (7) implies $\bar{u} \neq \bar{d}$. To allow for this MRS [9] parametrize

$$\bar{d} - \bar{u} = Ax^{-\alpha}(1-x)^{\beta_s}\,, \quad (8)$$

where $\alpha \simeq \alpha_M(0)$, since the difference may be associated with the lack of Regge $\rho - a_2$ exchange degeneracy. When this is done (sets D_0, D_-), it is found $\bar{d} > \bar{u}$ and that $I_{\rm GSR}$ of (6) is about 0.26. It is interesting to note that it is still possible to maintain $\bar{u} = \bar{d}$ and to obtain an equally good global description of deep-inelastic and related data but at the expense of a contrived small x behaviour of the valence distributions, see set S_0 of [9]. However it is more physical to allow $\bar{u} \neq \bar{d}$ and so the discussion will concentrate on sets D_0 and D_-. Fig. 4 summarizes the Gottfried sum rule discussion.

In addition to the parameters describing the input distributions there is the parameter $\alpha_s(M_Z^2)$ which specifies the QCD coupling and which determines the rate of evolution in Q^2. Using deep inelastic data we have

$$\begin{aligned}
&\alpha_s(M_Z^2) = 0.113 \pm 0.005 && \text{(BCDMS data [14])}\\
&\alpha_s(M_Z^2) = 0.111 \pm 0.006 && \text{(CCFR data [2])}\\
&\alpha_s(M_Z^2) = 0.112_5 \pm 0.005 && \text{(MRS global fit [8]).}
\end{aligned}$$

These determinations lie below, but are consistent with, the LEP value of

$$\alpha_s(M_Z^2) = 0.120 \pm 0.006 \quad \text{(LEP average [15]).}$$

In summary, MRS fit to deep inelastic and related data with a total of about 15 parameters. The quality of the fit is shown in Figs 5–8.

To determine $f_i(x, Q^2)$ from the evolution equations it is only necessary integrate from x up to 1. Thus the fits to the data do not involve, or determine, $f_i(x, Q^2)$ for values of x below that for which data exist. However the

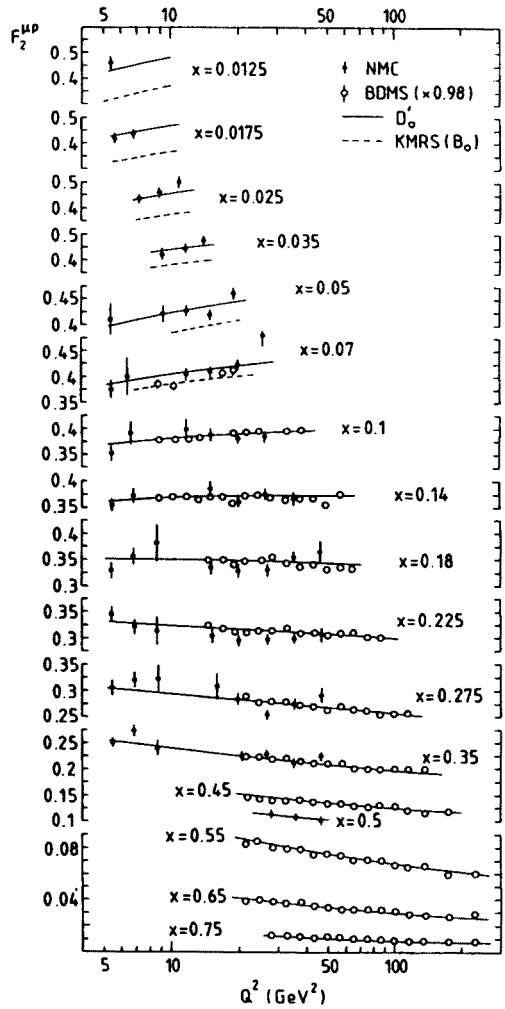

Fig. 5. The BCDMS [6] and NMC [1] measurements of $F_2^{\mu p}$, together with the description obtained in the global analyses of KMRS and MRS [8]. The NMC data were not available for KMRS. The figure is taken from Ref. [8].

precision of the data means that we should now have reliable sets of parton distributions at least in the region $x \gtrsim 0.02$. Extrapolations outside the region of the data are notoriously unreliable. All we can do is to use the input parametric forms, together with the evolution equations, to extrapolate to small x to show the general trends.

Fig. 9 shows parton sets D'_0 and D'_-; recall that the latter set incorporate the singular BFKL-like forms $xg, x\bar{q} \sim x^{-0.5}$ at small x. We see that

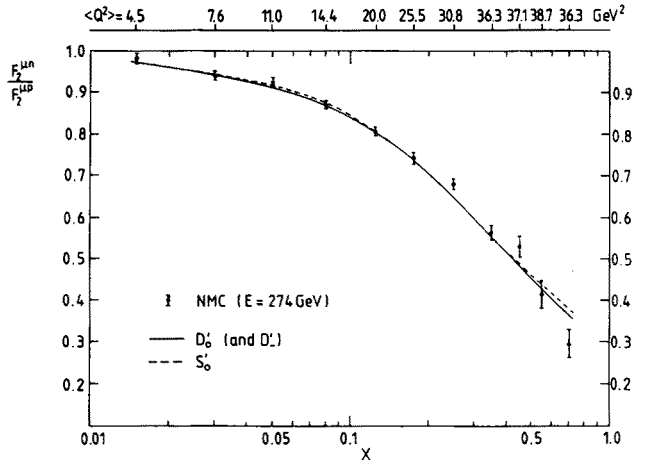

Fig. 6. The description of the NMC data [1] for the structure function ratio $F_2^{\mu n}/F_2^{\mu p}$ given by the S'_0, D'_0 and D'_- sets of partons [8]. The figure is taken from Ref. [8].

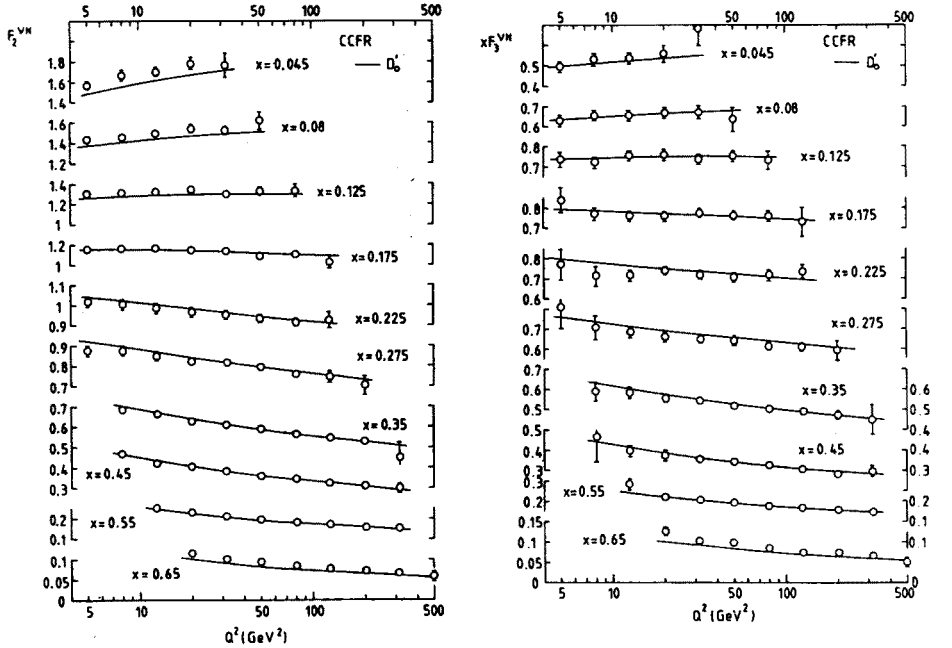

Fig. 7. The continuous curves show the description of the CCFR [2] measurements of $F_2^{\nu N}(x, Q^2)$ and $xF_3^{\nu N}(x, Q^2)$ by the D'_0 set of partons [8]. The data are shown after correction for the heavy target effects and after the overall renormalization of 0.95 required by the global fit, see Ref. [8].

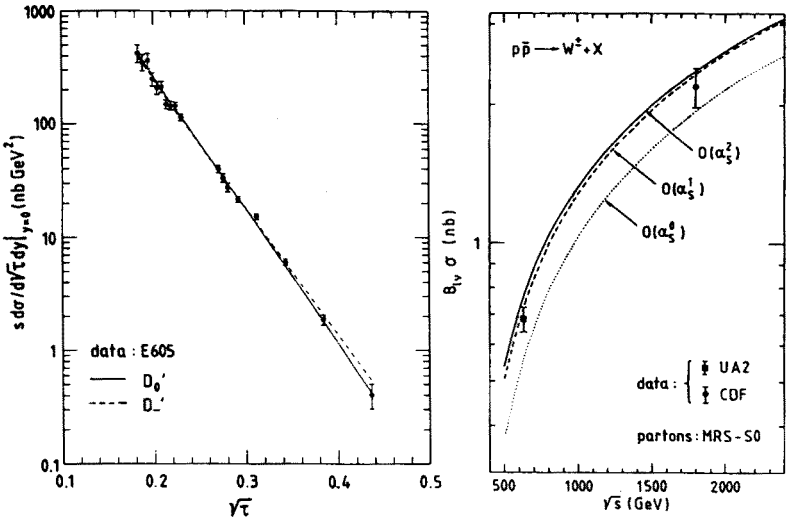

Fig. 8. The description of Drell-Yan and W production data obtained by the MRS partons of Ref. [8].

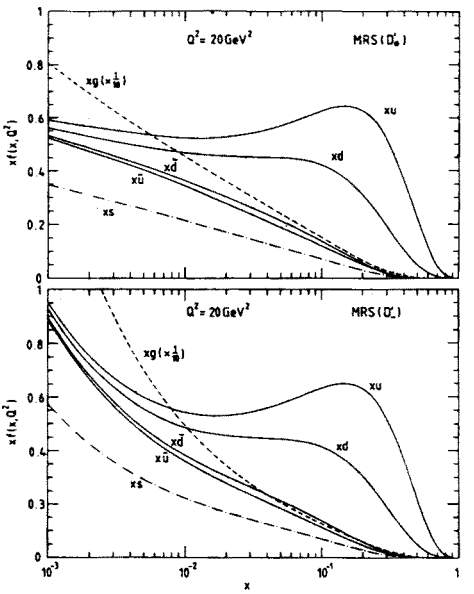

Fig. 9. The D_0' and D_-' sets [8] of parton distributions of the proton at $Q^2 = 20\text{GeV}^2$. Although the two sets are essentially identical in the x region of the data fitted ($x \gtrsim 0.02$) they differ greatly at small x due to the more singular (physically motivated) input forms used for the gluon and sea quarks in set D_-'.

the two sets are essentially identical for $x \gtrsim 0.02$ (though there is a little difference in the gluon that is necessary to conserve momentum), but they are dramatically different at small x. The recent HERA measurements of F_2^{ep} [4, 5] lie somewhat nearer to the D'_ extrapolation than to D'_0.

3. Summing leading logs: GLAP and BFKL equations

So far we have used the GLAP or Altarelli–Parisi equations to evolve up in Q^2 from a starting distribution at Q_0^2. For a non-singlet quark distribution the equation is of the form

$$\frac{\partial q(x,Q^2)}{\partial \log Q^2} = \frac{\alpha_s}{2\pi}\int_x^1 \frac{dy}{y} P_{qq}(\frac{x}{y}) q(y,Q^2) \equiv P_{qq} \otimes q\,. \tag{9}$$

To keep the discussion simple we consider just leading order and fixed, rather than running, coupling α_s. By rewriting (9) in terms of moments it is easy to show that the equation effectively sums the leading $(\alpha_s \log Q^2)$ contributions. The $(\alpha_s \log Q^2)^n$ contribution corresponds (in a physical or axial gauge) to the n-rung ladder diagram of Fig. 10 [16]. In fact this leading log arises from the strongly-ordered region of transverse momenta

$$Q^2 \gg k_{nT}^2 \gg \ldots k_{1T}^2 \gg Q_0^2\,.$$

Suppose now we wish to study the behaviour at small x. Then we encounter new logarithmic contributions of the form $(\alpha_s \log(1/x))^n$. These will need to be summed. First consider the case when

$$\alpha_s \log\frac{1}{x} \log\frac{Q^2}{Q_0^2} \simeq 1\,, \tag{10}$$

but where $\alpha_s \log(1/x)$ and $\alpha_s \log(Q^2/Q_0^2)$ are both small. At small x the gluon dominates and so we keep only $xg(x,Q^2)$. Now the leading

$$\left(\alpha_s \log\frac{1}{x} \log\frac{Q^2}{Q_0^2}\right)^n$$

contribution comes (in a physical gauge) from the n-rung ladder diagram where both the longitudinal and transverse momenta are strongly ordered as indicated in Fig. 11. Summing over these gluon ladders gives[2]

$$xg(x,Q^2) \sim \exp\left(2\left[\frac{3\alpha_s}{\pi}\log\frac{1}{x}\log Q^2\right]^{1/2}\right)\,, \tag{11}$$

[2] This form applies if $xg(x,Q_0^2) \sim$ constant. If $xg(x,Q_0^2) \sim x^{-1/2}$ say, then this singular behaviour is stable to evolution and overrides (11).

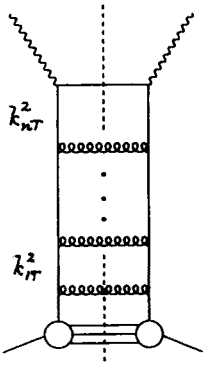

Fig.10

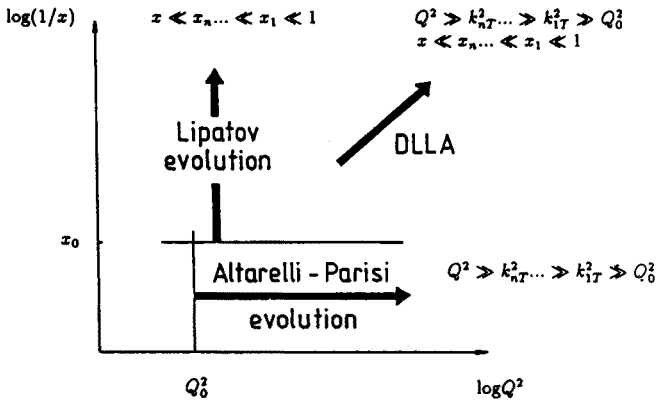

Fig.11

Fig. 10. The n-rung "ladder" diagram.

Fig. 11. The three different limits of $g(x, Q^2)$ in the $\log Q^2$, $\log(1/x)$ plane: *(i)* the leading $\log Q^2$ region where $\alpha_s \log Q^2 \sim 1$ but $\alpha_s \log(1/x)$ is small, reached by Altarelli–Parisi evolution from $g(x, Q_0^2)$ and $q(x, Q_0^2)$, *(ii)* the double leading log region where $\alpha_s \log Q^2 \log(1/x) \sim 1$ but $\alpha_s \log Q^2$ and $\alpha_s \log(1/x)$ are both small, and *(iii)* the leading $\log(1/x)$ limit where $\alpha_s \log(1/x) \sim 1$ but $\alpha_s \log Q^2$ is small, reached by evolution from $g(x_0, Q^2)$ using the Lipatov or BFKL equation. We also indicate the strongly-ordered regions of longitudinal and/or transverse parton momenta along the chain which give the leading log behaviours.

so that the gluon grows faster than any power of $\log(1/x)$ as x decreases. This is called the double leading log approximation or DLLA.

For HERA we need QCD predictions for small x but moderate Q^2. Starting from a knowledge of $g(x_0, Q^2)$ (with say $x_0 \gtrsim 0.01$) we wish to predict $g(x, Q^2)$ at smaller x, that is to evolve in the upwards direction in Fig. 11 at moderate Q^2. Therefore we must sum the leading $\log(1/x)$ terms but keep the full Q^2 dependence, not just the leading $\log(Q^2)$ terms. Clearly we must relax the strong ordering of the k_T's which gave the leading $\log(Q^2)$ behaviour, and integrate over the full k_T phase space. As in the other cases we can picture the leading $\log(1/x)$ behaviour as a sum of ladder diagrams, but now the QCD calculation is more involved. The resulting structure does indeed look like a summation of ladder diagrams but actually they are only an effective representation for a whole set of Feynman diagrams, which were originally summed by Lipatov and coworkers [3]. The $(\alpha_s \log(1/x))^n$ contribution comes from the n-rung diagram with strongly-ordered longitudinal momenta, see Fig. 11. The summation is effected by the Lipatov or BFKL

equation[3] which has the differential form

$$\frac{\partial f(x,k_T^2)}{\partial \log(1/x)} = \int dk_T'^2 K(k_T,k_T') f(x,k_T'^2)\,, \tag{12}$$

where $f(x,k_T^2)$ is the unintegrated gluon distribution in which the "last" k_T^2 integration along the ladder is unfolded

$$xg(x,Q^2) = \int^{Q^2} \frac{dk_T^2}{k_T^2} f(x,k_T^2)\,. \tag{13}$$

The full expression for the kernel K can be found in [3], or more recently in [18], for example. The BFKL equation, (12), can be written in the symbolic form

$$\frac{\partial f}{\partial \log(1/x)} = K \otimes f = \lambda f\,, \tag{14}$$

where λ are the eigenvalues of K. The solutions of (14) have the form $f \sim x^{-\lambda}$ and so the $x \to 0$ behaviour is controlled by the maximum eigenvalue of λ. For fixed α_s the leading small x behaviour can be found analytically. The maximum eigenvalue is

$$\lambda = \frac{3\alpha_s}{\pi} 4\log 2 \simeq 0.5\,. \tag{15}$$

This result is the motivation of the MRS(D$_-$) input small x behaviour with $\lambda_g = \lambda_{sea} = 0.5$.

It is worth looking at other features of the analytic form

$$\frac{f(x,k_T^2)}{(k_T^2)^{1/2}} \sim \frac{(x/x_0)^{-\lambda}}{[2\pi\lambda'' \log(x_0/x)]^{1/2}} \exp\left(\frac{-\log^2(k_T^2/\bar{k}_T^2)}{2\lambda'' \log(x_0/x)}\right) \tag{16}$$

with $\lambda'' = (3\alpha_s/\pi)28\zeta(3)$ where the Riemann zeta function $\zeta(3) = 1.202$. Form (16) displays another characteristic feature of the solution of the BFKL equation. Since there is no ordering in k_T there is a "random walk" in k_T as we proceed along the gluon chain and evolution to smaller x will be accompanied by a diffusion in k_T. Eq. (16) shows that the diffusion pattern is a Gaussian distribution in $\log k_T^2$ with a width that grows as $(\log(1/x))^{1/2}$

[3] More recently an alternative derivation has been given by Marchesini *et al.* [17], in which the virtual emissions are included by means of a non-Sudakov form factor. In this way they have obtained an equation which reduces to the BFKL equation at small x and to the Altarelli–Parisi equation at large x.

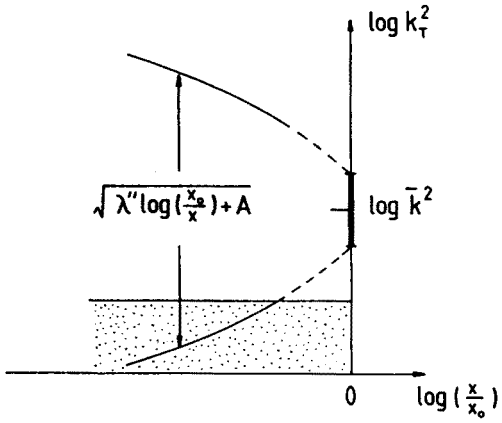

Fig. 12. The variation of the width of the Gaussian $\log k_T^2$ distribution of (16) as we use the BFKL equation to evolve down in x from a starting distribution at $x = x_0$ of width $\sim \sqrt{A}$. There is diffusion into the infrared region (shown dotted).

as x decreases, see Fig. 12. We foresee that diffusion will be a problem in the applicability of the BFKL equation since it can lead to an increasingly large contribution from the infrared (and ultraviolet) region of k_T^2 where the equation is not expected to be valid. We return to this discussion after we have introduced "shadowing".

4. Shadowing and the GLR equation

The increase $f \sim x^{-\lambda}$ or $xg \sim x^{-\lambda}$, as x decreases, cannot go indefinitely. If the density of gluons within the proton becomes too large they can no longer be treated as free partons. The growth, as $x \to 0$, must eventually be suppressed by gluon recombination. When do we expect the "shadowing" contributions to start to become appreciable? If we view the proton from a frame in which its momentum p is large, but in which $xp \gg Q$, then a measurement of $g(x, Q^2)$ probes a gluon of transverse size $\sim 1/Q$, but much smaller longitudinal size $\sim 1/px$, so that the proton appears as a thin disc. The number of gluons, n_g, per unit of rapidity is $xg(x, Q^2)$ and the gluon-gluon cross section $\hat{\sigma} \sim \alpha_s(Q^2)/Q^2$, so the crucial parameter is

$$W \equiv \frac{n_g \hat{\sigma}}{\pi R^2} \sim \frac{\alpha_s(Q^2)}{\pi R^2 Q^2} xg(x, Q^2), \tag{17}$$

where R is the radius of the proton. In regions of x and Q^2 where $W \ll 1$ the interaction between the gluons should be negligible. However at sufficiently

small x, when $W \sim \alpha_s$, we must allow for a suppression of the growth of the gluon density due to $2g \to g$ recombination. By considering QCD diagrams which become important at small x, recombination was estimated some time ago by Gribov, Levin and Ryskin [19], and a little later by Mueller and Qiu [20]. To a first approximation the normal evolution, Fig. 13(a), is corrected by including Fig. 13(b) (the so-called "fan" diagram) in which the gluon ladder branches into two ladders which couple to the proton.

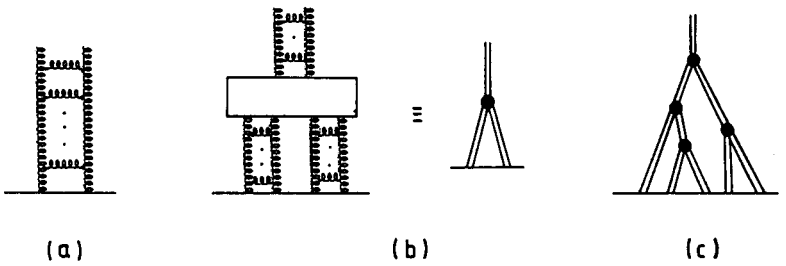

Fig. 13. (a) The type of ladder diagram associated with the BFKL "linear" evolution, (12), at small x; (b) the basic gluon shadowing or recombination diagram, also pictured as a "fan" diagram; (c) the sum of fan diagrams, such as the one shown, encapsulated in the "quadratic" GLR equation, (18).

The triple ladder vertex (shown as a rectangle) represents the sum of several (non-planar) diagrams. The iteration of this fan diagram produces a whole series of fan diagrams like the one shown in Fig. 13(c). In order to make progress GLR made simplifying assumptions: *(i)* for the form of the three-ladder vertex, *(ii)* that there are no correlations between the two gluon ladders (in Fig. 13(b)) which recombine and *(iii)* that the coupling of n gluon ladders to the proton is proportional to the n^{th} power of the single ladder coupling. In this way they were able to account for these shadowing effects by including an additional term in the BFKL equation, (14), so that

$$\frac{\partial f(x,k_T^2)}{\partial \log(1/x)} = K \otimes f - \frac{81\alpha_s^2(k_T^2)}{16R^2k_T^2}[xg(x,k_T^2)]^2 . \tag{18}$$

The minus sign and the quadratic nature of the extra term reflect the suppression of growth of f, as x decreases, due to gluon recombination. The equation is known as the GLR equation [19].

Recently Bartels [21], and subsequently Levin *et al.* [22], have found assumption *(ii)* is not valid. There is a coupling ($\sim 1/N_c^2 \sim 10\%$) between the ladders, which effectively increases the shadowing term by a factor of about 1.7 [23]. This result calls the validity of the GLR equation into

doubt, although it is probably still reasonable to use the "enhanced" form of (18) to estimate the onset of shadowing. Clearly the GLR equation is only applicable in the region where $W \lesssim O(\alpha_s)$, see Fig. 14. From (17) we see that as Q^2 increases shadowing becomes less important.

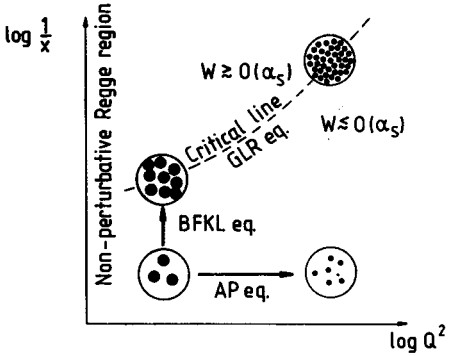

Fig. 14. The (x, Q^2) regions of validity of the various evolution equations. The gluonic content of the proton (as resolved by a Q^2 probe) is also indicated. Perturbative QCD is applicable below the critical line.

Quantitatively the crucial "shadowing" parameter in (18) is R. It says how the gluons are concentrated within the proton. The conventional assumption is that they are uniformly spread across the proton; then R is the proton radius (~ 5 GeV^{-1}). However it has been advocated that they may be concentrated in "hot-spots" within the proton, so analyses are also often performed with $R = 2$ GeV^{-1}. The numerical studies [24] of shadowing effects using (18) indicate that the kinematic regime accessible at HERA is well below the critical line and the shadowing will be small, unless "hot-spots" exist.

5. Small x physics: some applications of the BFKL equation

The resummation of gluon ladders, $f(x, k_T^2)$, is a universal ingredient in the perturbative QCD predictions of all small x processes driven by the gluon. For example $f(x, k_T^2)$ occurs in the calculation of the structure functions; of deep-inelastic events with jets; of heavy quark-pair, J/ψ and prompt photon production; as well as deep inelastic diffraction at small x.

Recently there have been several studies of the properties of the solutions $f(x, k_T^2)$ of the BFKL equation [18, 24–27]. In some cases numerical solutions have been obtained. The usual technique is to solve the differential form of the equation, (12) (or (18)), by step-by-step integration down in x from an input distribution $f(x_0, k_T^2)$, at say $x_0 = 0.01$, determined from the gluon of one of the parton sets of Section 2. Running α_s and the effects of

shadowing have been incorporated [18, 24, 27]. There are different treatments of the infrared region. We can impose a simple lower-limit cut-off k_0^2 on the $k_T'^2$ integration of (12), or, better, we can introduce a physically motivated parametric from $f(x, k_T^2) \sim k_T^2/(k_T^2 + k_a^2)$ below k_0^2 [27]. For a given value of k_T^2, the characteristic behaviour $f(x, k_T^2) \sim Cx^{-\lambda}$ soon sets in with decreasing x. The normalization of the solution C is found to be much more sensitive to the infrared region than is the value of λ. Indeed for $k_0^2 \simeq 1$ GeV^2 we find that $\lambda \simeq 0.5$, essentially independent of the value of k_T^2 and only weakly dependent on k_0^2 (or k_a^2).

5.1. *QCD prediction of F_2 at small x*

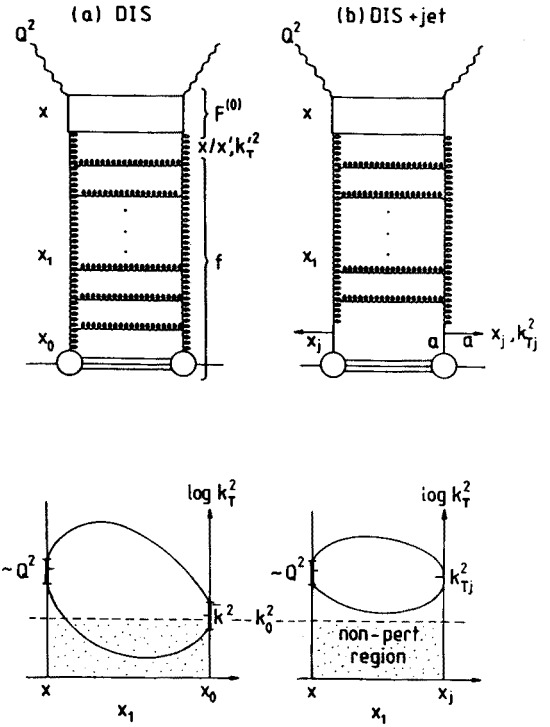

Fig. 15. The upper diagrams show the gluon ladder contributions to small x (a) deep inelastic scattering and (b) together with an energetic jet. The lower sketches show the variation of the width of the $\log k_T^2$ diffusion patterns as we proceed along the ladder.

At small x, say $x \sim 10^{-3}$, the deep inelastic probe dominantly interacts with a sea quark and so, to leading order, the structure function $F_2(x, Q^2)$ reflects the small x behaviour of the sea quark distributions. Since the

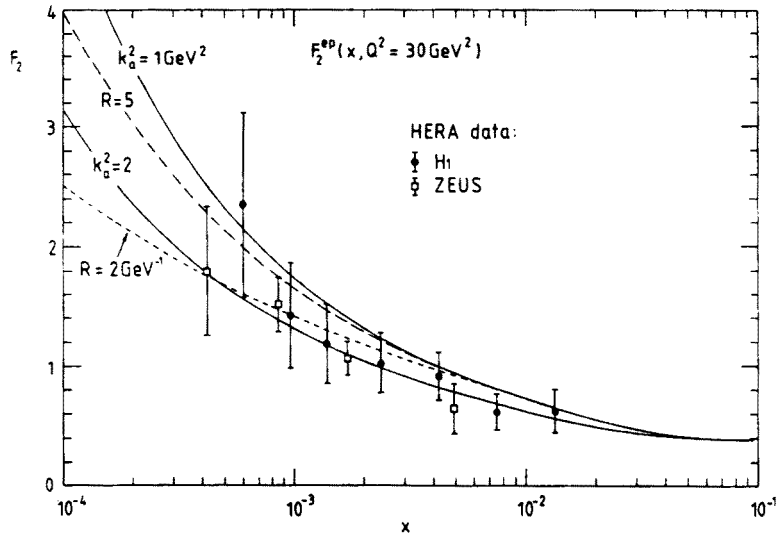

Fig. 16. The perturbative QCD predictions for $F_2(x, Q^2)$ obtained [27] from the k_T factorization formula (20). The continuous curves correspond to the infrared parameter $k_a^2 = 1$ and 2 GeV^2, and the dashed curves show the suppression caused by conventional and "hot-spot" shadowing for $k_a^2 = 1$ GeV^2. The data are from H1 [4] and ZEUS [5].

density of gluons increases rapidly with decreasing x, the sea quark distributions are themselves increasingly dominated by the gluon distribution, via $g \to q\bar{q}$. This component may be calculated in perturbative QCD. The relevant diagram is shown in Fig. 15(a). According to k_T-factorization, the contribution is of the form

$$F_2(x, Q^2) = \int_x^1 \frac{dx'}{x'} \int \frac{dk_T^2}{k_T^4} f(\frac{x}{x'}, k_T^2) F_2^{(0)}(x', k_T^2, Q^2), \qquad (19)$$

where x/x' is the longitudinal momentum fraction carried by the gluon which dissociates into the $q\bar{q}$ pair. The function $F^{(0)}$ corresponds to the calculable quark box (and cross box) shown in the upper part of Fig. 15(a). The perturbative QCD prediction [27] for F_2^{ep} is compared with the recent HERA data in Fig. 16. We see that, up to an overall (infrared cut-off dependent) normalization, the QCD predictions [27] are in excellent agreement with the data. The comparison suggests that HERA may have obtained the first evidence of the BFKL growth coming from the resummation of soft gluons.

The variation of the width of the k_T diffusion pattern, as x_1 varies between x (where the width is given by the quark box) and x_0 (controlled

by the gluon input), is sketched in the lower part of Fig. 15(a). Even for large Q^2, the boundary conditions at x_0 mean that the non-perturbative infrared region is penetrated, which is reflected in the infrared sensitivity of the normalization of F_2 shown in Fig. 16.

5.2. Deep inelastic events with a measured jet

Mueller [28] has emphasized the special features of deep inelastic (x, Q^2) events which contain a measured jet (x_j, k_{Tj}^2) in the kinematic regime where *(i)* the transverse momentum of the jet satisfies $k_{Tj}^2 \simeq Q^2$, *(ii)* the jet longitudinal momentum, x_j, is as large as is experimentally feasible ($x_j \sim 0.1$), and *(iii)* $z = x/x_j$ is small. A diagrammatic representation of the process is shown in Fig. 15(b); for "large" x_j strong-ordering at the parton a-gluon vertex should be a good approximation. The beauty of this measurement in that attention is focussed directly on the BFKL $z^{-\lambda}$ type behaviour at small z arising from the resummation of soft gluon emissions. The choice $k_{Tj}^2 \simeq Q^2$ neutralizes the ordinary gluon radiation which would have arisen from the Altarelli–Parisi evolution in Q^2. The differential structure function has a leading small z behaviour of the form [29]

$$x_j \frac{\partial F_2}{\partial x_j \partial k_{Tj}^2} \simeq \alpha_s(Q^2) \left[\sum_a x_j f_a(x_j, k_{Tj}^2) \right] z^{-\lambda}, \tag{20}$$

where $\sum f_a = g + \frac{4}{9}(q + \bar{q})$ is known from the global parton analyses. This observable contains the anticipated $z^{-\lambda}$ behaviour, where, as before, λ is the maximum eigenvalue of the BFKL kernel, and so, in principle, it should allow an unambiguous identification of λ.

Another advantage of this process is that we can choose $k_{Tj}^2 \simeq Q^2$ sufficiently large so as to minimize the k_T diffusion into the infrared region; see the diffusion pattern sketched in Fig. 15(b), or calculated in Ref. [26].

6. Polarized structure function measurements

This year has also seen the measurement of the polarized structure function g_1 of the deuteron by SMC [30] and the neutron by E142 [31], to complement the earlier measurement of g_1 for the proton by EMC [32]. The measurements may be used to determine

$$I^i \equiv \int_0^1 g_1^i(x) dx, \tag{21}$$

for $i = p, n, d$, and hence to test the fundamental Bjorken sum rule

$$I^p - I^n = \frac{1}{6}\frac{g_A}{g_V}\left(1 - \frac{\alpha_s(Q^2)}{\pi} + \ldots\right) + \text{higher twist}. \qquad (22)$$

Ellis and Karliner [33] show that both the new SMC and E142 measurements, when combined with EMC, are compatible with the Bjorken sum rule provided the Q^2 dependence is taken into account. (Some adjustment of their higher twist contribution is still necessary [34].)

The "spin crisis" dates to when only I_p was measured. With an additional assumption that the strange sea within the proton is unpolarized, Ellis and Jaffe [35] were then able to predict I^p and I^n separately, and also the fraction of the proton's spin carried by the quark constituents (namely $\Delta q = 0.58$). The "old" EMC measurement of I^p disagreed with the Ellis-Jaffe prediction by some 2.5 standard deviations, and moreover implied $\Delta q \sim 0$. This is so-called "spin crisis". Close and Roberts [36] have translated all 3 experiments to $Q^2 = 5$ GeV^2 and used updated input wherever possible to produce the comparison shown in the Table below.

	Ellis-Jaffe pred.	Experiment ($\rightarrow Q^2 = 5$ GeV^2)	Δq
I^p	0.172 ± 0.009	EMC: 0.135 ± 0.011	0.21 ± 0.11
I^n	-0.018 ± 0.009	E142: -0.028 ± 0.006	0.49 ± 0.06
I^d	0.077 ± 0.009	SMC: 0.041 ± 0.016	0.24 ± 0.15

The spread of values and the uncertainties are too large to be sure whether or not there is a spin crisis. Clearly the "ball is in the experimentalists court". SMC will improve their statistics and will measure I^p. Experiments have been approved at SLAC (E143) and at HERA (Hermes) to measure both I^p and I^n.

7. Conclusions

It has been a vintage year for deep inelastic scattering. The great improvement in fixed target data mean parton distributions should be reliable for $x \gtrsim 0.02$, though further information on the gluon is urgently needed. The dramatic rise of F_2 observed at HERA is suggestive of the effect of soft gluon resummation. However experiment and theory for small x are in their infancy, and we can look forward to much progress in this area. This year has also seen a rekindling of interest in polarization structure functions with the promise of definitive data for both the proton and neutron in the near future.

I thank Jan Kwieciński, Dick Roberts, James Stirling, Peter Sutton and Adrian Askew for enjoyable collaborations on the subject of this review. I also thank the Institute of Nuclear Physics in Kraków for their warm hospitality and the European Community for a "Go-East" Fellowship.

REFERENCES

[1] NMC: P. Amaudruz *et al.*, *Phys. Lett.* **B259**, 159 (1992).
[2] CCFR collaboration: S.R. Mishra, *Proc. of Lepton-Photon Symposium*, Geneva 1991; P.Z. Quintas *et al.*, *Phys. Rev. Lett.* **71**, 1307 (1993).
[3] E.A. Kuraev, L.N. Lipatov, V.S. Fadin, *Sov. Phys. JETP* **45**, 199 (1977); Ya.Ya. Balitsky, L.N. Lipatov, *Sov. J. Nucl. Phys.* **28**, 822 (1978).
[4] H1 collaboration: I. Abt *et al.*, *Nucl. Phys.* **B407**, 515 (1993).
[5] ZEUS collaboration: M. Derrick *et al.*, *Phys. Lett.* **B316**, 412 (1993).
[6] BCDMS collaboration: A.C. Benvenuti *et al.*, *Phys. Lett.* **B223**, 485 (1989).
[7] WA70 collaboration: M. Bonesini *et al.*, *Z. Phys.* **C38**, 371 (1988).
[8] A.D. Martin, W. J. Stirling, R.G. Roberts, *Phys. Lett.* **B306**, 145 (1993).
[9] A.D. Martin, W.J. Stirling, R.G. Roberts, *Phys. Rev.* **D47**, 867 (1993).
[10] CTEQ collaboration: J. Botts *et al.*, *Phys. Lett.* **B304**, 159 (1993).
[11] A.D. Martin, W. J. Stirling, R.G. Roberts, *J. Phys. G* **19**, 1429 (1993).
[12] CCFR collaboration: A.O. Bazarko *et al.*, *Nevis report* **1492**, March 1993; see also C. Foudas *et al.*, *Phys. Rev. Lett.* **64**, 1207 (1990); S.A. Rabinowitz *et al.*, *Phys. Rev. Lett.* **70**, 134 (1993).
[13] NMC: P. Amaudruz *et al.*, *Phys. Rev. Lett.* **66** 2712 (1991); E.M. Kabuss, *Nucl. Phys.* B (Proc. Supp.) **29A**, 1 (1992); M. Arneodo *et al.*, CERN preprint PPE/93-117, (1993).
[14] M. Virchaux, A. Milsztajn, *Phys. Lett.* **B272**, 221 (1992).
[15] The LEP collaborations, CERN preprint PPE/93-157, (1993).
[16] G. Altarelli, *Phys. Rep.* **81**, 1 (1982).
[17] S. Catani, F. Fiorani, G. Marchesini, *Nucl. Phys.* **B336**, 18 (1990); S. Catani, F. Fiorani, G. Marchesini, G. Oriani, *Nucl. Phys.* **B361**, 645 (1991); G. Marchesini, *Proc. of Workshop "QCD at 200 TeV", Erice, Italy, June 1990,* eds L. Cifarelli and Yu. L. Dokshitzer, Plenum Press, 1992, p.183
[18] J. Kwieciński, A.D. Martin, P.J. Sutton, *Phys. Rev.* **D44**, 2640 (1991); *Phys. Lett.* **B264**, 199 (1991).
[19] L.V. Gribov, E.M. Levin, M.G. Ryskin, *Phys. Rep.* **100**, 1 (1983).
[20] A.H. Mueller, J. Qiu, *Nucl. Phys.* **B268**, 427 (1986).
[21] J. Bartels, *Phys. Lett.* **B298**, 204 (1993); DESY preprint 93-028, (1993).
[22] E.M. Levin, M.G. Ryskin, A.G. Shuvaev, *Nucl. Phys.* **B387**, 589 (1992).
[23] J. Bartels, M.G. Ryskin, DESY preprint 93-081, (1993).
[24] A.J. Askew, J. Kwieciński, A.D. Martin, P.J. Sutton, *Phys. Rev.* **D47**, 3775 (1993).

[25] E.M. Levin, G. Marchesini, M.G. Ryskin, B.R. Webber, *Nucl. Phys.* **B357**, 167 (1991); J.R. Forshaw, P.N. Harriman, *Phys. Rev.* **D46**, 3778 (1992); J.C. Collins, P.V. Landshoff, *Phys. Lett.* **B276**, 196 (1992); R.E. Hancock, D.A. Ross, *Nucl. Phys.* **B383**, 575 (1992); J.R. Forshaw, P.N. Harriman, P.J. Sutton, Manchester preprint M/C-TH 93/14, (1993).

[26] J. Bartels, H. Lotter, *Phys. Lett.* **B309**, 400 (1993).

[27] A.J. Askew, J. Kwieciński, A.D. Martin, P.J. Sutton, Durham preprint DTP/93/38, (*Mod. Phys. Lett.* in press); Durham preprint DTP/93/28, September 1993.

[28] A.H. Mueller, *Nucl. Phys.* B (Proc. Supp.) **18C**, 125 (1990); *J. Phys. G* **17**, 1443 (1991).

[29] J. Bartels, A. De Roeck, M. Loewe, *Z. Phys.* **C54**, 635 (1992); *Nucl. Phys.* B (Proc. Supp.) **29A**, 61 (1992); W.-K. Tang, *Phys. Lett.* **B278**, 363 (1992); J. Kwieciński, A.D. Martin, P.J. Sutton, *Phys. Rev.* **D46**, 921 (1992); *Phys. Lett.* **B287**, 254 (1992); *Nucl. Phys.* B (Proc. Supp.) **29A**, 67 (1992).

[30] SMC: B. Adeva *et al.*, *Phys. Lett.* **B302**, 533 (1993).

[31] SLAC-E142: P.L. Anthony *et al.*, *Phys. Rev. Lett.* **71**, 959 (1993).

[32] EMC: J. Ashman *et al.*, *Phys. Lett.* **B206**, 364 (1988); *Nucl. Phys.* **B328**, 1 (1989).

[33] J. Ellis, M. Karliner, *Phys. Lett.* **B313**, 131 (1993).

[34] I.I. Balitsky, V.M. Braun, A.V. Kolesnichenko, erratum MPI-Ph/93-00 to *Phys. Lett.* **B242**, 245 (1990).

[35] J. Ellis, R.L. Jaffe, *Phys. Rev.* **D9**, 1444 (1974).

[36] F.E. Close, R.G. Roberts, RAL preprint 93-040, (1993).